

RSC Advances



This is an *Accepted Manuscript*, which has been through the Royal Society of Chemistry peer review process and has been accepted for publication.

Accepted Manuscripts are published online shortly after acceptance, before technical editing, formatting and proof reading. Using this free service, authors can make their results available to the community, in citable form, before we publish the edited article. This *Accepted Manuscript* will be replaced by the edited, formatted and paginated article as soon as this is available.

You can find more information about *Accepted Manuscripts* in the [Information for Authors](#).

Please note that technical editing may introduce minor changes to the text and/or graphics, which may alter content. The journal's standard [Terms & Conditions](#) and the [Ethical guidelines](#) still apply. In no event shall the Royal Society of Chemistry be held responsible for any errors or omissions in this *Accepted Manuscript* or any consequences arising from the use of any information it contains.

ARTICLE

Self-assembling Morphologies of Symmetric PS-*b*-PMMA in Different Sized Confining Grooves

Cite this: DOI: 10.1039/x0xx00000x

Wenhui Chen^a, Jun Luo^{*a}, Peixiong Shi^b, Chunlong Li^a, Xiaobin He^a, Peizhen Hong^a, Junfeng Li^a and Chao Zhao^{*a}

Received 00th January 2014,

Accepted 00th January 2014

DOI: 10.1039/x0xx00000x

www.rsc.org/

As an emerging lithographical technique, DSA has drawn increasingly attentions due to numerous advantages such as low cost, high throughput and convenience on processing. However, there are still some challenges confronted with DSA, including defects control, complex patterns fabrication and pattern registration. In this work, self-assembling morphologies of a lamellar diblock copolymer (BCP) PS-*b*-PMMA are investigated to gain more understanding of the DSA progress and to offer some reference for pattern transfer process. Quantized number of lines in directing grooves are achieved, while warps and dislocations appear when the number of lines jumps from n to $n+1$. Another key finding of this work is that, gradient variations on line width are observed near the edge of the confining grooves, which shows ununiformity of the patterns. A novel structure model is proposed to interpret the variation of the BCP lines. All these finds in this work provide valuable information and insight for nanowires patterning by DSA in the state-of-the-art semiconductor devices.

Introduction

As the sizes of semiconductor devices continuously decrease, conventional optical lithography has almost reached its limits due to the increasingly cost and more complicated processes. According to the international technology roadmap for semiconductors (ITRS, 2013 edition)¹, directed self-assembly (DSA) of block copolymer (BCP), as well as extreme ultra-violet lithography (EUVL)²⁻⁴, nanoimprint lithography (NIL)⁵⁻⁷ and maskless lithography⁸, has been recommended as a potentially available lithography method to satisfy the requirements of resolution and pattern quality in the 16/14 nm and beyond complementary metal-oxide-semiconductor transistor (CMOS) technology nodes. In this context, DSA technique using BCP material is emerging as a competitive candidate for lithography in the future⁹.

The BCP is a special material, which is composed of two or more chemically distinct and covalently linked blocks. For example, poly(styrene-*b*-methyl methacrylate) (PS-*b*-PMMA) consisting of two monomers (PS and PMMA) is the most popular BCP due to its good compatibility with semiconductor fabrication. After annealing, the blocks in the BCP would phase separate from each other and self-assemble into the most energetically favorable nanostructures¹⁰. By orienting these small sized nanopatterns, uniform long-ordered line/space or hole arrays can be obtained and used as etching masks in nanofabrication¹¹⁻¹⁷. This patterning technique is called DSA. It is a novel “bottom-up” lithographic technology¹⁸, which differs a lot from conventional “top-down” approaches. DSA utilizes pre-patterned substrates with chemical heterogeneities¹⁹⁻²¹, topographic features²²⁻²⁵ or both^{26, 27} to direct BCP into ordered patterns. The size of the patterns formed by DSA depends on the length of the BCP

molecule chains, which is highly uniform and determined by the block volume fractions and the degree of polymerization of the BCP. Chemoepitaxy and graphoepitaxy are now two main ways for BCP directing. Chemoepitaxy, in which one-block-wetting stripes/dots embedded in neutral substrate is used to direct BCP, can offer high-density pattern arrays with no space sacrifice^{28, 29}, while it is more complex and challenging in fabrication and pattern registration. On the other hand, graphoepitaxy uses topographic features to direct BCP from sidewalls with neutral substrates^{30, 31}, which differs a lot from bottom-directing chemoepitaxy method, has the benefits of process simplicity, flexibility for pattern placement and high potential degree of frequency multiplication.

As an emerging lithographic technology of low cost and high throughput, DSA has attracted enormous interests of researchers. However, there are still many challenges which obstruct it to become a usable manufacturing technique. Firstly, defect density has to be controlled within a low level for manufacturing use³². Dislocation is one of the most common types of defects in DSA, and there is still no perfect solution to eliminate it. Secondly, DSA now can only produce simple periodic patterns, thus design rules of chip layouts have to be modified for the compatibility with DSA³³⁻³⁶. Thirdly, pattern placement or registration is a serious concern. Especially in graphoepitaxy directing method, the morphology of the BCP will be closely related to the commensurability between the size of the directing features and the natural bulk period of the BCP (L_0). Some investigations on pattern placement and elasticity of the cylindrical BCP in nanogrooves have been performed^{37, 38}. It was demonstrated that the cylindrical BCP patterns would be compressed or stretched to conform the width of the directing groove. However, to the lamellar BCP, such a systematic research on its self-assembling

morphologies and pattern registration in nanogrooves is rarely explored.

In this work, a systematic investigation on symmetric PS-*b*-PMMA self-assembling properties in directing grooves is carried out. In particular, the commensurability between the size of the directing groove and the self-assembling morphology of the PS-*b*-PMMA is studied to get more understanding on how the PS-*b*-PMMA behaves in certain sized confinement. Different sized hydrogen silsesquioxane (HSQ) grooves are prepared on neutralized substrate by e-beam lithography (EBL). HSQ has been shown to be a very suitable material for directing in DSA technique^{31, 39}, because it can transform into silica under high temperatures. Silica is a very common material in semiconductor and can be removed by HF solutions easily^{40, 41}. After spin-coating the PS-*b*-PMMA into HSQ grooves and annealing, phase-separated lines can be achieved. Scanning electron microscope (SEM) images of these samples are processed and analyzed using a customized Matlab script to get detailed information of BCP lines. It will be valuable for researchers to study the morphologies of the lines for the pattern transfer process from the BCP layer to the substrate.

Experimental

Materials

Random copolymer Poly(styrene-co-methylmethacrylate-co-hydroxyethyl methacrylate), denoted as P(S-*r*-MMA-*r*-HEMA) ($M_n = 35600$ kg/mol, PDI = 1.28, PS mole fraction = 57%, HEMA mole fraction = 2%), and symmetric block copolymer Poly(styrene-*b*-methyl methacrylate), denoted as PS-*b*-PMMA ($M_n = 22000$ - b - 22000 kg/mol, PDI = 1.09), were purchased from Polymer Source Inc. and used without any further purification. HSQ electron beam spin-on resist (XR-1541) was purchased from Dow Corning and used as received.

Neutral layer preparation

4-inch bare Si(100) wafers with approximately 1.5-nm-thick native oxide were first immersed into piranha solutions (30% H₂O₂/H₂SO₄ 1:5 v/v) at 120 °C for 15 min, then rinsed with DI water and dried under N₂ flow to remove any organic contamination and to increase the concentration of hydroxyl groups on the surface for neutral layer graft. Random copolymer P(S-*r*-MMA-*r*-HEMA) solutions of 0.5wt% in toluene were spin-coated on the cleaned wafers at 3000 rpm for 60 s to get ~25-nm-thick RCP layers which are equally chemical preferential to PS and PMMA. Subsequently, the samples were annealed in an oven at 240 °C for 5 min under N₂ atmosphere to graft chains of P(S-*r*-MMA-*r*-HEMA) onto the hydroxyl functionalized surface. Ungrafted polymers were washed away with toluene under ultrasonication for 1 min. After that, the wafers were dried under N₂ flow to remove any residual toluene, so that a neutral layer of ~5 nm thickness on the wafer was obtained.

Directing features fabrication

After neutral layer preparation, HSQ e-beam resist XR-1541 was spin-coated onto the wafers at 3000 rpm for 60 s to get a resist film of 40 nm thickness. Following this, annealing the wafers on a hot plate at 100 °C for 3 min and 200 °C for 3 min respectively was performed as post exposure bake process (PEB) of the resist. Then the wafers were exposed by a e-beam of 10 mC cm⁻² and

developed in MF CD26+4%NaCl solutions at 33.5 °C for 60 s, followed by rinsing in DI water and drying in N₂ to produce grooves of different widths varying from 25 to 200 nm with a 5 nm interval.

BCP film preparation

Symmetric PS-*b*-PMMA solutions of 0.5wt% in toluene were spin-coated onto the surface of HSQ patterned wafers at 3000 rpm for 60 s to deposit the BCP into the grooves. The wafers were then annealed in an oven at 240 °C for 5 min under N₂ atmosphere to evaporate remaining solvent and induce phase separation of the PS-*b*-PMMA.

Characterization

A Hitachi S-5500 scanning electron microscope (SEM) was used for collecting images at an accelerating voltage of 1 kV. To get original morphologies of BCP films, we did not perform any other process such as plasma etching or sputtering metal on the samples to enhance the contrast. The SEM images were processed by Matlab with the image processing toolbox to obtain the widths of the grooves, the sizes of the BCP lines and the cross-sectional structures of the patterns.

Result and discussion

Figure 1 shows schematically the process flow for graphoeptaxial DSA, including preparation of the neutral layer, patterning of the HSQ resist and DSA of PS-*b*-PMMA in nanogrooves. Firstly, the random copolymer P(S-*r*-MMA-HEMA) was spin-coated on wafers and annealed to graft the polymer chains to the surface, then ungrafted polymers were removed by washing in toluene to obtain a chemically neutral film to both PS and PMMA, shown in Figure 1(i, ii, iii). Secondly, HSQ resist was spin-coated on the neutralized substrate and patterned by EBL to produce nanogrooves as directing features, shown in Figure 1(iv, v, vi). Thirdly, the block copolymer PS-*b*-PMMA was spin-coated into the HSQ grooves and annealed at a temperature above the glass transition temperature of the PS-*b*-PMMA to induce phase separation of the BCP, shown in Figure 1(vii, viii).

Thirty six different sized grooves varying from 25 to 200 nm with 5 nm interval were fabricated. SEM images of these samples, as shown in Figure 2, display self-assembling morphologies of PS-*b*-PMMA in these grooves. Two different morphologies are observed, which are, perpendicular lines to the confining sidewalls in the grooves of 25 nm and 30 nm width, and parallel lines to the confining sidewall in the grooves of 35 nm and above width. This phenomenon agrees well with the theoretical conclusion reported by Walton *et al.*⁴² To achieve the lowest free energy, there is a critical number of layers of the lamellar BCP between two parallel confining walls, below that the morphology can be either perpendicular or parallel to confining walls depending on the extent of chain deformation, and above that the parallel morphology is always favored over the perpendicular one.

The number of the lines (n) in each groove is plotted against the normalized groove width (W_g/L_0) in Figure 3(a), where W_g is the average width of the groove which is determined by processing and measured in SEM images with Canny edge detection in Matlab. L_0 is the natural bulk period which is 25 nm in the lamellar PS-*b*-PMMA. Clearly, the number of the lines in the

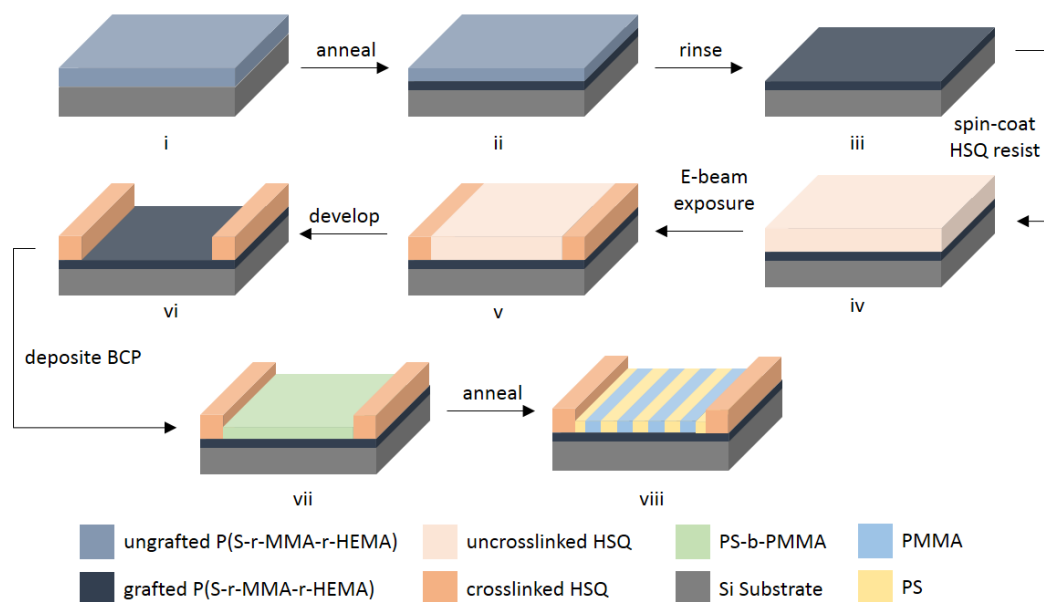


Figure 1. Schematic representation of the process flow for graphoepitaxial DSA of PS-b-PMMA. (i) P(S-r-MMA-r-HEMA) film deposition on the Si substrate. (ii) Graft of the random copolymer. (iii) Removal of ungrafted polymers. (iv) HSQ resist deposition on the neutral layer. (v) Exposure of HSQ resist with e-beam. (vi) Development of HSQ resist. (vii) PS-b-PMMA deposition into HSQ grooves. (viii) Phase separation of PS-b-PMMA by annealing.

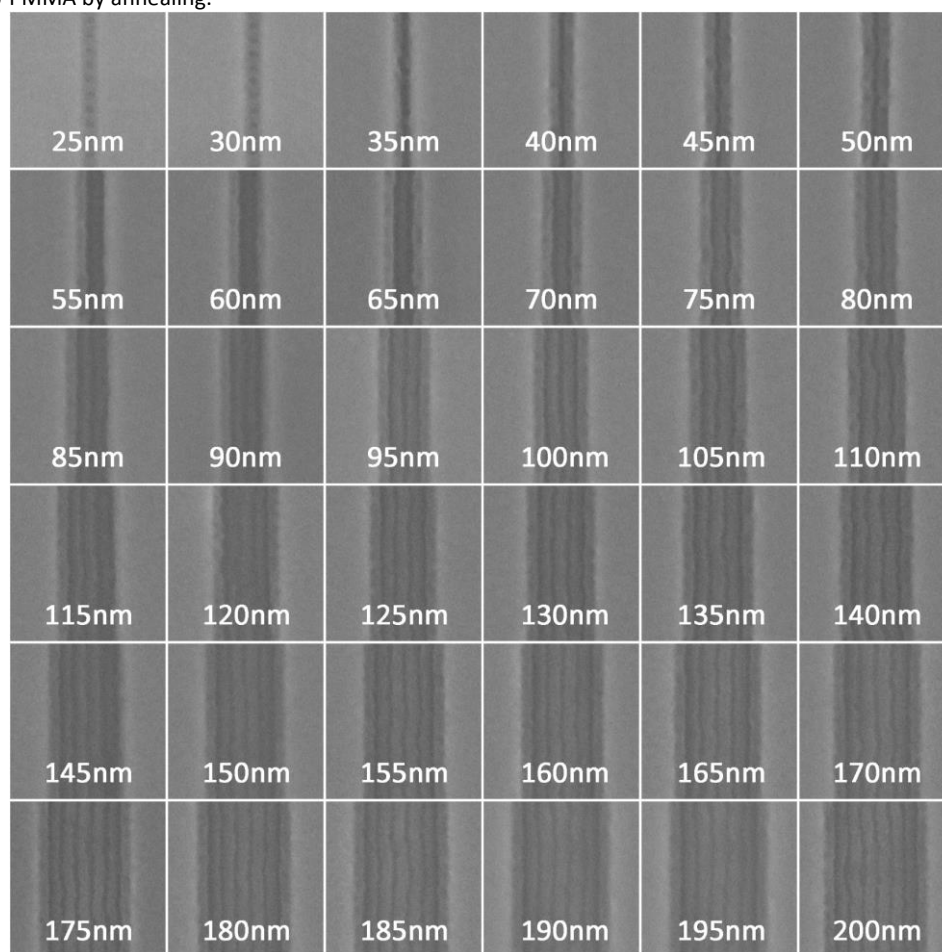


Figure 2. SEM images of PS-b-PMMA self-assembling morphologies in different sized HSQ grooves. The labels on the images indicate the widths of the grooves which were designed in the e-beam exposing layout.

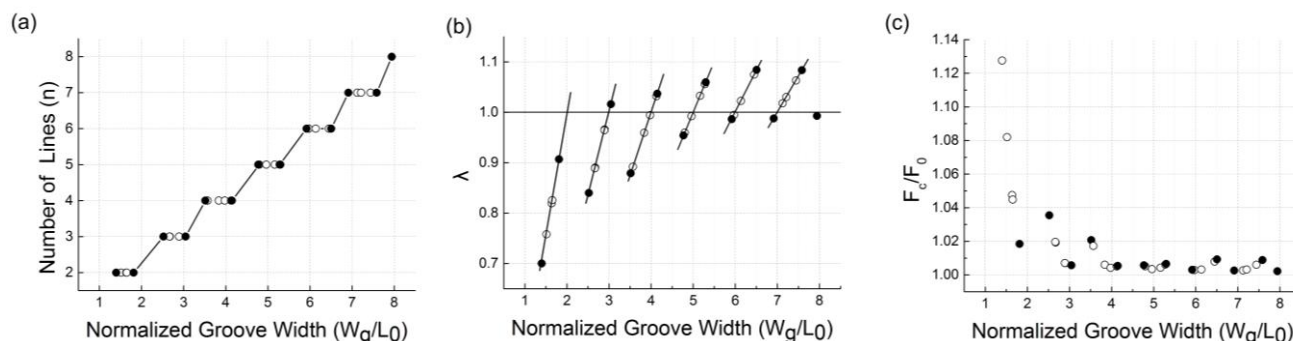


Figure 3. Variation of three parameters of the PS-b-PMMA against the normalized groove width. (a) Number of lines. (b) Normalized period that indicates the degree of compression or expansion of BCP lines. (c) The ratio between the free energy per polymer chain of the confined PS-b-PMMA and that of the unconfined PS-b-PMMA. The black dots represents the grooves with widths near the transition points from n to $n+1$ lines.

grooves is quantized to achieve a stair-like curve, which indicates that n is stable in each corresponding range of the groove width. BCP lines are compressed or stretched to comply with the groove width. The degree of compression or expansion of the BCP lines can be modelled by considering the normalized period λ , which is given by equation (1). Figure 3(b) shows the variation of λ against the normalized groove width. While the groove width (W_g) is less than the integral times of the bulk equilibrium period (nL_0), the BCP is compressed, otherwise it is stretched.

$$\lambda = \frac{W_g}{nL_0} \quad (1)$$

Cheng *et al.* reported that, to a cylindrical BCP, a transition in the number of rows from n to $n+1$ occurs when $W_g \approx (n+0.5)L_0$, which can be demonstrated by finding the lowest free energy of the confined polymer system³⁸. Here in the lamellar BCP, the similar thresholds of the groove width for the transition from n to $n+1$ lines are also observed. The ratio between the free energy per polymer chain of the confined BCP (F_c), and the free energy per polymer chain of the unconfined bulk BCP (F_0) is approximated as a function of λ in equation (2) and equation (3), where γ_{AS} is the interfacial tension between block A and the confining sidewall, γ_{AB} is the interfacial tension between block A and block B, proposed by Turner *et al.*⁴³ To demonstrate the minimum of the free energy, these ratios are calculated and plotted in Figure 3(c), which clearly shows that, to each certain number of lines, the minimum of the ratio is at the integral

normalized groove width, while the transition from n to $n+1$ lines occurs when W_g/L_0 is near $n+0.5$.

$$\frac{F_c}{F_0} = \frac{1}{3} \left[\lambda^2 + \frac{2}{\lambda} + \frac{2\Gamma}{n\lambda} \right] \quad (2)$$

$$\Gamma = \frac{\gamma_{AS}}{\gamma_{AB}} \quad (3)$$

Another interesting phenomenon observed is that some defects such as warps and dislocations occur when the groove width is near the transition point from n to $n+1$, as the black dots in Figure 3. SEM images of these grooves are shown in Figure 4. These imperfect patterns may be caused by the high free energy of the confined polymer system around the transition point. When the groove width is near the transition point, the free energy of the BCP system is high enough so that the BCP lines are sensitive to the edge roughness of the confining sidewalls. As the edge of the sidewall cannot be perfectly smooth, a little bump on the sidewall may induce warps of the BCP lines, which may even develop into dislocations.

To obtain more details of the self-assembling morphology of BCP lines in confining grooves, SEM images of higher resolution were processed in Matlab. Figure 5 shows a schematic of how a SEM image is processed. Here, a ~ 200 -nm-wide groove with 8 BCP lines inside is chosen as an example. Firstly, the specified region of a groove in the SEM image is cut out and then noise-smoothed by a median filter. A cross-sectional view of the groove is extracted and plotted out, with the number of pixels as

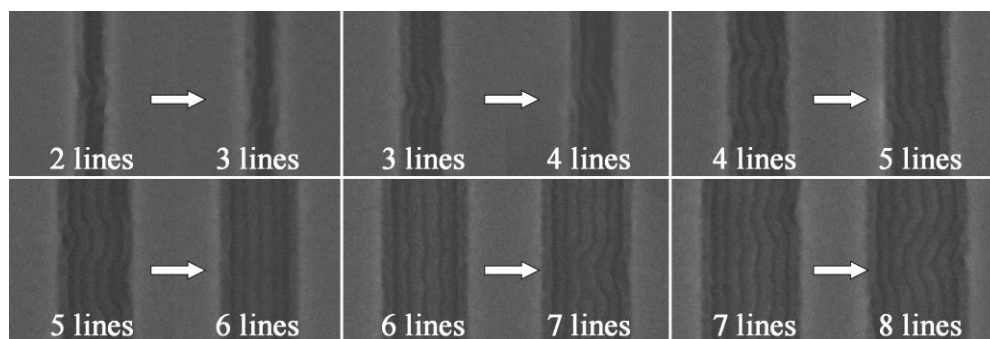


Figure 4. Defects of the BCP in the grooves with widths near the transitioning points from n to $n+1$ lines.

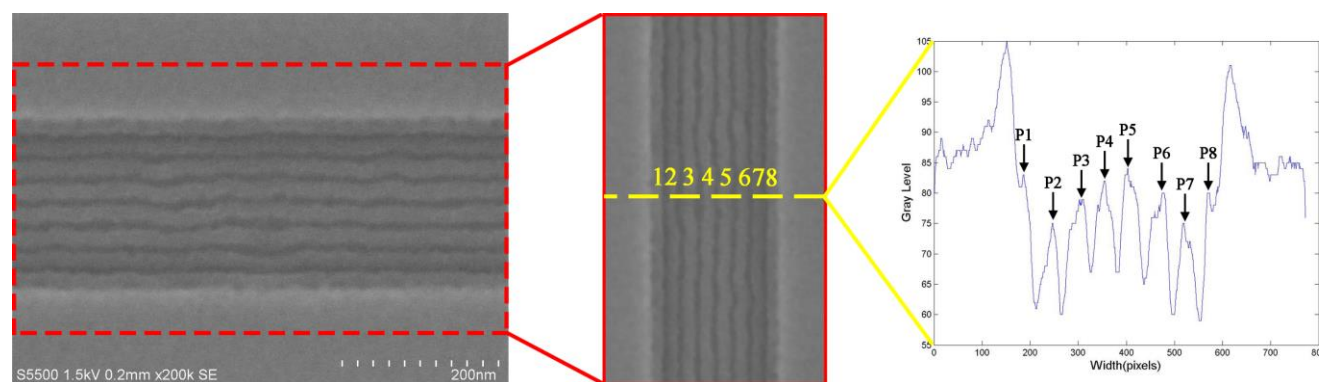


Figure 5. Schematic showing the procedure of the SEM image processing in Matlab. In the right image, the horizontal axis is the number of the pixel across the groove (0.4960938nm/pixel), and the vertical axis is the gray level of each pixel. The 8 peaks (P1~P8) in the right image correspond to the 8 bright lines in the middle and left images.

the horizontal axis and the gray level as the vertical axis. Each pixel in the SEM image corresponds to 0.4960938 nm length at $\times 200\text{k}$ magnification according to the reporting file of the SEM system. The right image in Figure 5 clearly shows 8 full peaks (P1~P8) corresponding to the 8 bright lines in the original SEM image. Since the width of a peak (W_p) is defined as the distance between the bottoms of nearby two valleys, the widths of every lines can be measured by data cursor in Matlab, then calculated and recorded in Table 1. It is apparent that lines at the edge of the groove (line 1, 2, 7, 8) is narrower than those in the center (line 3, 4, 5, 6).

Table 1. Widths of BCP lines in a 199.4nm groove cross section

Line Order	1	2	3	4	5	6	7	8
Width(nm)	18.4	25.8	29.3	28.3	30.3	30.8	24.8	13.9

Considering the randomness of one sample, a few SEM images were processed and measured to find whether there is an universal law in every groove. Seven SEM images of grooves whose designed widths are 75 nm , 100 nm , 125 nm , 150 nm , 175 nm , 200 nm were chosen, and several number of cross sections of the grooves were cut out in each image to measure the average values of line widths. These average widths are plotted in Figure 6 and fitted into smooth curves. It is clearly shown that lines in the groove center are generally wider than those near the groove

edge. According to the difference in width, these lines can be classified into three levels, as shown by the 3 red frames in Figure 6. Lines in level 1 are those closest to the confining sidewalls, whose widths are from 15 to 22 nm . Lines in level 2 are those secondly closest to the confining sidewalls, whose widths are from 23 to 28 nm . Except these lines in level 1 and 2, all other lines in the groove are classified into level 3 with width in the range of $29\sim 32\text{ nm}$. Since the natural bulk period of the PS-*b*-PMMA in the experiment is 25 nm , it can be concluded with cautions that lines in level 1 are compressed, and lines in level 3 are stretched, while lines in level 2 are slightly compressed or stretched depending on the groove width.

For insurance of the representativeness of these average values, a statistical analysis was performed on the data points. Firstly, in each SEM image, 10 cross sections at intervals of 50 nm were chose to get 10 samples for each line. The standard deviations of these samples were calculated and plotted in Figure 7(a). It can be obtained from Figure 7(a) that, standard deviations of these samples all locate in the range of 0.8 nm to 3.1 nm . which is about equal to the line edge roughness (LER) of commonly used e-beam resists, while some fluctuations may appear due to process variations and image noises⁴⁴. Secondly, the number of samples along each groove was increased from 10 to 20 and 40, at intervals of 25 nm and 12.5 nm respectively. their standard

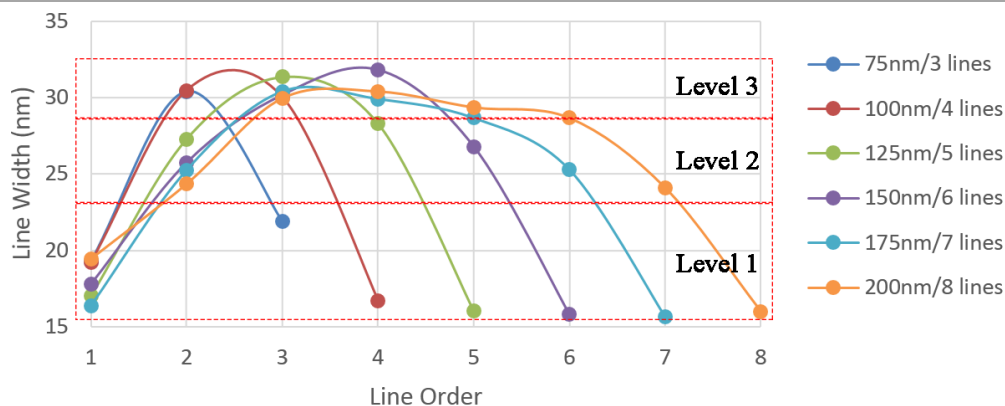


Figure 6. Average widths of lines in different sized grooves. Lines in confining grooves are classified into there levels. Level 1 contains the lines firstly closest to the sidewalls with widths between 15 nm and 22 nm . Level 2 contains the lines secondly closest to the sidewalls with width between 23 nm and 28 nm . All the other lines in the center are classified into level 3 whose widths are between 29 nm and 32 nm .

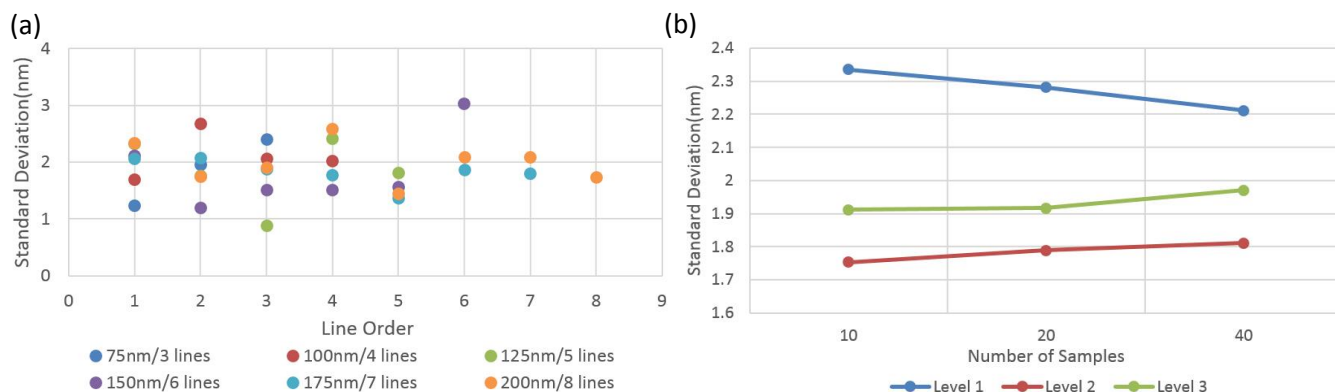


Figure 7. Statistical analysis for samples of line widths. (a) Distribution of standard deviations for 10 sample data points along each groove. All the standard deviations locate in the range from 0.8nm to 3.1nm. (b) Variations of standard deviations for 10, 20 and 40 sample data points along three different-level lines. The standard deviations decrease (Level 1) or increase (Level 2 and Level 3) slightly with variations less than 0.1 nm.

deviations were compared, as shown in Figure 7(b). Here three different-level lines in the 200nm/8lines were chose as an example to observe the variation of standard deviation versus the number of sample data points. As the number of the sample data points doubles and quadruples, the standard deviations of the three different-level lines increase (Level 1) or decrease (Level 2, Level 3) slightly, with negligible variations of 0.1 nm or less. Therefore, it can be concluded that with the increasing number of sample data points, no obvious variation on the standard deviation is observed, which means, 10 sample data points at intervals of 50 nm along each groove are representable for the average line width characterization.

By analyzing the widths of the lines, the structures of BCP lines can be described by the model elucidated in Figure 7. When the groove can only accommodate 3 lines, the pattern structure is 1-3-1 with no lines in level 2 (Figure 7(a)). When the groove is wider for accommodating 4 lines, the pattern structure becomes

1-3-3-1 (Figure 7(b)). As the groove becomes even wider for accommodating 5 lines, two lines in level 2 are added in and the groove becomes continuously wider for accommodating 5 lines, 6 lines and above, more lines in level 3 are added into the center of the groove, with no change in the pattern structures at the edge, which are always the gradient 1-2-3 (Figure 7(d)(e)). Therefore, there is always an axisymmetric structure of BCP lines in the confining groove, where widths of the lines are gradient near the groove edge and approximately equal in the groove center. This phenomenon is similar with what has been reported by Cheng *et al.* that gradient variation in domain size and spacing of cylindrical BCP across the groove was observed, which can be utilized to realize gradient nanostructures³⁷. The reason for the variation of the groove widths near the edge is that, the HSQ sidewalls have more stronger affinities to PS than PMMA³¹, which decreases the concentration of PS blocks in the vicinity of the edge. This indicates that the surface chemistry of the confining sidewalls affects pattern formation over several

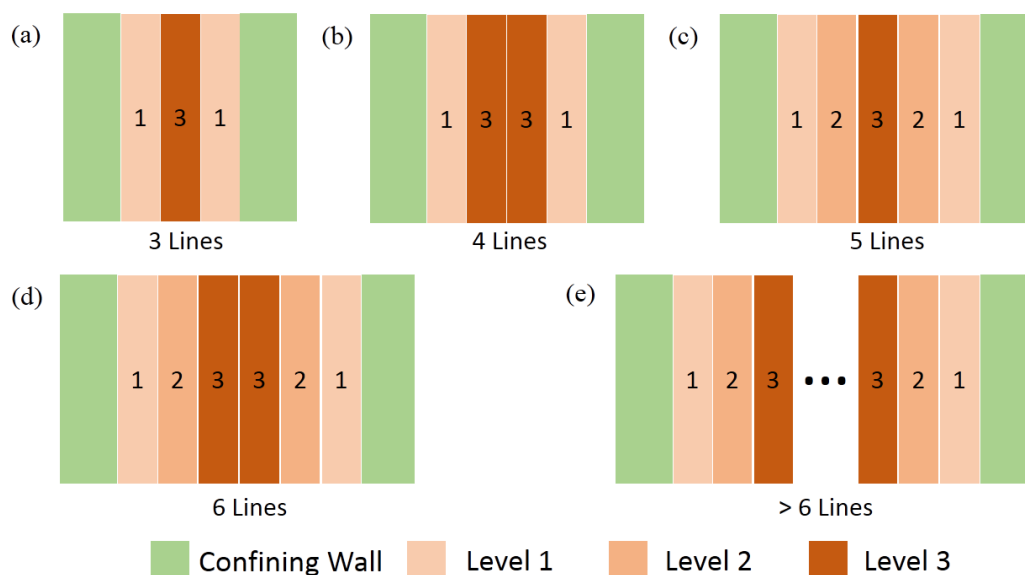


Figure 8. Models of lamellar BCP line structures between two parallel confining walls. (a) 1-3-1 structure in the groove with 3 lines. (b) 1-3-3-1 structure in the groove with 4 lines. (c) 1-2-3-2-1 structure in the groove with 5 lines. (d) 1-2-3-3-2-1 structure in the groove with 6 lines. (e) the universal structure in the groove with more than 6 lines, widths of lines are gradient at the edge and approximately equal in the center.

periods³⁷. Therefore, by adjusting the confining groove widths or tuning the surface chemistry of the sidewalls, gradient nanostructures can be fabricated.

The foregoing results show a detailed morphology of the lamellar PS-*b*-PMMA in confining grooves, which is a nonuniform structure that lines in the center are stretched while lines at the edge are compressed. This may be caused by the different affinities of two blocks to confining sidewall. It is worth noting that, more research work should be performed further to eliminate the non-uniformity in BCP lines, because sizes of lines and spaces are compulsory to be highly equal to guarantee small variation of device performance thus excellent product yield in integrated circuit (IC) technology.

Conclusions

This work focus on the self-assembling morphologies of the lamellar block copolymer PS-*b*-PMMA (22k-*b*-22k) in directing grooves. Different sized HSQ grooves on neutralized Si substrate were fabricated for directing self-assembly of BCP. Both perpendicular and parallel phase-separated lines of BCP to the sidewalls were observed in the grooves of different widths. Several key findings are summarized as what follows: (1) The number of lines in parallel structures was demonstrated to be quantized in terms of the commensurability between the groove width (W_g) and the BCP bulk period (L_0); (2) Around the transition point from n to $n+1$ lines, some defects like wraps and dislocations occur in the BCP patterns due to the high sensibility of the patterns to the edge roughness of the confining walls, which is caused by the high free energies of the polymer system in those states; (3) A gradient variation of the line width from the edge to the center of grooves is observed, which is believed to be the result of the interfacial interaction between the blocks and the confining sidewalls. A novel structure model was proposed to interpret these findings and to harvest more understanding on the sizes and positions of the lines in grooves. This research offers a detailed reference on pattern registration of graphoepitaxial DSA technique, which have particular significance for the subsequent pattern transfer process, because sizes of lines and spaces in semiconductor devices should be controlled precisely to guarantee small variation of device performance thus excellent product yield in integrated circuit (IC) technology. More research should be carried out to obtain more understandings on the mechanism of the width variation for BCP lines in grooves, and to develop the corresponding pattern transfer process for DSA technique.

Acknowledgements

The authors would like to thank Xiaosa Zhang from Chanchun Institute of Applied Chemistry, Chinese Academy of Sciences and Pengfei Nan from Fudan University for helpful discussions.

Notes and references

^a Key Laboratory of Microelectronics Devices & Integrated Technology, Institute of Microelectronics, Chinese Academy of Sciences, Beijing 100029, P. R. China

^b DANCHIP, Technical University of Denmark, DK 2800, Lyngby, Denmark

1. <http://www.itrs.net/Links/2013ITRS/Summary2013.htm>.
2. J. W. Thackeray, R. A. Nassar, K. Spear-Alfonso, R. Brainard, D. Goldfarb, T. Wallow, Y. Wei, W. Montgomery, K. Petrillo, O. Wood, C.-s. Koay, J. Mackey, P. Naulleau, B. Pierson and H. H.

3. Solak, *Journal of Photopolymer Science and Technology*, 2007, 20, 411-418.
4. J. Benschop, V. Banine, S. Lok and E. Loopstra, *J Vac Sci Technol B*, 2008, 26, 2204-2207.
5. B. Paeivaenranta, A. Langner, E. Kirk, C. David and Y. Ekinci, *Nanotechnology*, 2011, 22.
6. M. D. Austin, H. X. Ge, W. Wu, M. T. Li, Z. N. Yu, D. Wasserman, S. A. Lyon and S. Y. Chou, *Applied Physics Letters*, 2004, 84, 5299-5301.
7. L. J. Guo, *Advanced Materials*, 2007, 19, 495-513.
8. H. Schift, *J Vac Sci Technol B*, 2008, 26, 458-480.
9. R. Menon, A. Patel, D. Gil and H. I. Smith, *Materials Today*, 2005, 8, 26-33.
10. S.-J. Jeong, J. Y. Kim, B. H. Kim, H.-S. Moon and S. O. Kim, *Materials Today*, 2013, 16, 468-476.
11. F. S. Bates and G. H. Fredrickson, *Annual Review of Physical Chemistry*, 1990, 41, 525-557.
12. S. Kim, D. O. Shin, D. G. Choi, J. R. Jeong, J. H. Mun, Y. B. Yang, J. U. Kim, S. O. Kim and J. H. Jeong, *Small*, 2012, 8, 1563-1569.
13. S.-J. Jeong, H.-S. Moon, J. Shin, B. H. Kim, D. O. Shin, J. Y. Kim, Y.-H. Lee, J. U. Kim and S. O. Kim, *Nano letters*, 2010, 10, 3500-3505.
14. J. Y. Cheng, C. A. Ross, E. L. Thomas, H. I. Smith and G. J. Vancso, *Applied Physics Letters*, 2002, 81, 3657.
15. K. W. Guarini, C. T. Black, Y. Zhang, H. Kim, E. M. Sikorski and I. V. Babich, *Journal of Vacuum Science & Technology B: Microelectronics and Nanometer Structures*, 2002, 20, 2788.
16. C. T. Black and O. Bezenecenet, *Ieee T Nanotechnol*, 2004, 3, 412-415.
17. Y.-H. La, E. W. Edwards, S.-M. Park and P. F. Nealey, *Nano letters*, 2005, 5, 1379-1384.
18. B. Rathsack, M. Somervell, J. Hooge, M. Muramatsu, K. Tanouchi, T. Kitano, E. Nishimura, K. Yatsuda, S. Nagahara, I. Hiroyuki, K. Akai and T. Hayakawa, *Alternative Lithographic Technologies Iv*, 2012, 8323, 83230B-83230B-83214.
19. K. Koo, H. Ahn, S.-W. Kim, D. Y. Ryu and T. P. Russell, *Soft Matter*, 2013, 9, 9059-9071.
20. M. P. Stoykovich, H. Kang, K. C. Daoulas, G. Liu, C.-C. Liu, J. J. de Pablo, M. Müller and P. F. Nealey, *Acs Nano*, 2007, 1, 168-175.
21. J. Y. Cheng, C. T. Rettner, D. P. Sanders, H.-C. Kim and W. D. Hinsberg, *Advanced Materials*, 2008, 20, 3155-3158.
22. R. Ruiz, H. Kang, F. A. Detcheverry, E. Dobisz, D. S. Kercher, T. R. Albrecht, J. J. de Pablo and P. F. Nealey, *Science*, 2008, 321, 936-939.
23. Y. Jung & Park, *Journal of Materials Chemistry C*, 2013, 1, 4020-4024.
24. S. M. Park, M. P. Stoykovich, R. Ruiz, Y. Zhang, C. T. Black and P. F. Nealey, *Advanced Materials*, 2007, 19, 607-611.
25. S. J. Jeong, J. E. Kim, H. S. Moon, B. H. Kim, S. M. Kim, J. B. Kim and S. O. Kim, *Nano letters*, 2009, 9, 2300-2305.
26. E. Han, H. Kang, C. C. Liu, P. F. Nealey and P. Gopalan, *Advanced Materials*, 2010, 22, 4325-4329.
27. S. J. Jeong and S. O. Kim, *J Mater Chem*, 2011, 21, 5856-5859.
28. D. Ok & Shin, B. Hoon & Kim, H. Min & Jin, M. Gyu & Lee and S. Ouk & Kim, *J Mater Chem*, 2012, 22, 6307-6310.
29. P. A. R. Delgadillo, R. Gronheid, C. J. Thode, H. Wu, Y. Cao, M. Neisser, M. Somervell, K. Nafus and P. F. Nealey, *J Micro-Nanolith Mem*, 2012, 11.
30. R. Gronheid, L. Van Look, P. R. Delgadillo, I. Pollentier, Y. Gao, G. Lin and P. F. Nealey, *Journal of Photopolymer Science and Technology*, 2013, 26, 147-152.
31. D. P. Sanders, J. Cheng, C. T. Rettner, W. D. Hinsberg, H.-C. Kim, H. Trung, A. Fritz, S. Harer, S. Holmes and M. Colburn, *Journal of Photopolymer Science and Technology*, 2010, 23, 11-18.
32. D. Borah, S. Rassapa, M. T. Shaw, R. G. Hobbs, N. Petkov, M. Schmidt, J. D. Holmes and M. A. Morris, *Journal of Materials Chemistry C*, 2013, 1, 1192-1196.
33. C. Yi, H. YoungJun, P. R. Delgadillo, N. Vandenbroeck, R. Gronheid, C. Boon Teik, Y. Hashimoto, A. Romo, M. Somervell, K. Nafus and P. F. Nealey, *Proceedings of the SPIE - The International Society for Optical Engineering*, 2013, 8680, 86801S (86807 pp.)-86801S (86807 pp.).

33. J. Qin, G. S. Khaira, Y. Su, G. P. Garner, M. Miskin, H. M. Jaeger and J. J. de Pablo, *Soft Matter*, 2013, 9, 11467-11472.
34. H. S. P. Wong, C. Bencher, H. Yi, X. Y. Bao and L. W. Chang, *Alternative Lithographic Technologies Iv*, 2012, 8323, 832303-832303-832307.
35. H. Yi, X. Y. Bao, J. Zhang, C. Bencher, L. W. Chang, X. Chen, R. Tiberio, J. Conway, H. Dai, Y. Chen, S. Mitra and H. S. Wong, *Adv Mater*, 2012, 24, 3107-3114, 3082.
36. T. R. Younkin, R. Gronheid, P. R. Delgadillo, B. T. Chan, N. Vandebroek, S. Demuyne, A. Romo-Negreira, D. Parnell, K. Nafus, S. Tahara and M. Somervell, *Advances in Resist Materials and Processing Technology Xxx*, 2013, 8682.
37. J. Y. Cheng, C. A. Ross, E. L. Thomas, H. I. Smith and G. J. Vancso, *Advanced Materials*, 2003, 15, 1599-+.
38. J. Y. Cheng, A. M. Mayes and C. A. Ross, *Nature materials*, 2004, 3, 823-828.
39. R. Tiron, X. Chevalier, S. Gaugiran, J. Pradelles, H. Fontaine, C. Couderc, L. Pain, C. Navarro, T. Chevolleau, G. Cunge, M. Delalande, G. Fleury and G. Hadziioannou, *Alternative Lithographic Technologies Iv*, 2012, 8323.
40. J. K. Yang, B. Cord, H. Duan, K. K. Berggren, J. Klingfus, S.-W. Nam, K.-B. Kim and M. J. Rooks, 2009.
41. M. Rommel and J. Weis, *J Vac Sci Technol B*, 2013, 31, 06F102.
42. D. Walton, G. Kellogg, A. Mayes, P. Lambooy and T. Russell, *Macromolecules*, 1994, 27, 6225-6228.
43. M. Turner, *Physical Review Letters*, 1992, 69, 1788-1791.
44. G. P. Patsis, V. Constantoudis, A. Tserepi, E. Gogolides and G. Grozev, *Journal of Vacuum Science & Technology B*, 2003, 21, 1008-1018.